High sensitivity ammonia detection using metal nanoparticles decorated on graphene macroporous frameworks/polyaniline hybrid

Fatemeh Ahmadi Tabr[a], Farah Salehiravesh[a], Hossein Adelnia[b], Jaber Nasrollah Gavgani[a,*], Mojtaba Mahyari[c,*]

[a] Department of Polymer Engineering and Color Technology, Amirkabir University of Technology, P.O. Box 15875-4413, Tehran, Iran
[b] Australian Institute for Bioengineering and Nanotechnology, University of Queensland, Brisbane, Australia
[c] Malek-Ashtar University of Technology, P.O. Box 16765-3454, Tehran, Iran

ABSTRACT

In this paper, we presented the fabrication and properties of new ammonia (NH_3) sensors with sensitive layer of nickel nanoparticles decorated on three-dimensional nitrogen-doped graphene-based frameworks/polyaniline (NiNPs@3D-(N)GFs/PANI) hybrid. The hybrid are synthesized through in-situ oxidative polymerization on flexible thin substrate. Synergetic behavior between both components manifested outstanding sensitivity (750.2 at 1000 ppm NH_3) and quick response (95 s) and recovery (25 s) times and a lower limit of detection (~ 45 ppb) at room temperature. The sensitivity of NiNPs@3D-(N)GFs/PANI hybrid sensor was shown to be about 14 times more than its of pure PANI sensor at 1000 ppm of NH_3. The excellent sensitivity of the as-prepared hybrid is mainly originated from the substantial rise of hole-like carriers by NiNPs@3D-(N)GFs as well as improved inter-molecule interactions via π- π electron networks. The obtained results revealed significant advantages for the synthesized hybrid sensor, making it a suitable choice for real-world applications of NH_3 detection.

1. Introduction

As an inorganic component, ammonia (NH_3) is widely employed in many industries just like food processing, medical prognosis, agriculture, refrigeration systems, etc. However, exposure to even low concentrations of NH_3, adversely affects the human health [1,2]. Accordingly, development of highly sensitive, durable, and economical devices for ammonia detection is of outmost importance. Among various techniques for NH_3 detection, chemical sensors have recently been introduced as one of the most efficient and inexpensive methods with fast response and high sensitivity.

Recently, many efforts have been made to investigate potential materials for NH_3 detection. Among the considered materials as sensing layer of NH_3 sensor, metal oxides such as WO_3, ZnO, In_2O_3, and etc. have demonstrated low sensitivity at high temperatures (> 300 °C) [3–6]. On the other hand, conductive polymers such as polyaniline have widely been utilized as sensing materials due to their low fabrication cost and sensing performance to NH_3 gas at room temperature [7–10]. However, their performance as practical sensors in real industrial applications is limited due to several downsides, including low sensitivity and thermal stability. Hence, it is of much importance to design sensors with proper materials to operate under harsh environmental conditions.

Graphene as innovative carbonic substance have attracted more attention as qualified substitutes for electronic applications [11–15]. For instance, the outstanding properties like high electrical conductivity and large surface area presented by graphene [16,17] have led to its acceptable sensitivity regarding any adsorbed/desorbed molecules [18]. Until now, ones have pulled off in their desperate attempts to improve performance of conventional graphene-based ammonia sensors [19]. The surface area of the sensing materials can directly affect the extent of ammonia sensitivity. Therefore, the efficiency of sensors can be improved significantly by enhancement of specific surface area via architectural and morphological modification of graphene. Three-dimensional graphene-based architectures are excellent candidates to be used as porous matrix for accepting metal nanoparticles, metal oxides, and active conductive polymers for high ammonia detection [20–23]. Moreover, the sensitivity of graphene and consequently, the amount of adsorbed/desorbed molecules on it can be improved by surface modification approaches such as chemical doping with nitrogen atoms [24,25].

In this study, the chemical oxidative synthesis of nickel nanoparticles decorated on three-dimensional nitrogen-doped graphene-based frameworks/polyaniline (NiNPs@3D-(N)GFs/PANI) hybrid as sensing material on flexible and highly transparent polyethylene

---

* Corresponding authors.
  E-mail addresses: jnasrollah@aut.ac.ir, jnasrollah@gmail.com (J.N. Gavgani), m_mahyari@sbu.ac.ir (M. Mahyari).

terephthalate thin film for NH_3 detection has been investigated. In addition, it has been indicated that such inexpensive flexible NiNPs@ 3D-(N)GFs/PANI devices can also be utilized for chemical sensing with high sensitivity, low response and recovery times, a lower limit of detection as well as excellent reversibility.

2. Experimental procedure

2.1. Materials

Aniline monomer and ammonium persulfate with high purity (99.9%) were prepared from Fluka Co. Aniline was applied after twice distillation under vacuum situation in order to eliminate impurities. Other chemicals were used up as-received a ready supply of Aldrich. Deionized (DI) water was applied for all experiments.

2.2. Synthesis of graphene oxide (GO)

GO was fabricated according to the reformed Hummers approach, using expanded graphite (EG) [23,26]. The solution of EG (1 g) and sulfuric acid (200 mL) was mixed in a three-necked flask. After that, $KMnO_4$ (10 gr) was dropped to the above solution. The resulted solution mixture was then moved to an ice bath. The color of obtained solution mixture was significantly changed to light brown after slow incorporation of H_2O_2 solution (50 mL in 200 mL DI water) through 30 min. Then GO particles were purified by centrifugation with a HCl solution (9:1 volumetric ratio, water: HCl). A value ranging 5–6 was achieved for the pH of solution via repeating the centrifuging and washing with DI water. Finally, DI water was added to dilute the GO dispersion and afterwards, the GO particles were softly shaken to become exfoliated.

2.3. Procedures for synthesis of the three-dimensional nitrogen-doped graphene-based frameworks (3D-(N)GFs)

A hydrothermal process followed by freeze drying was employed for prepartion of 3D-(N)GFs [27]. Briefly, dicyandiamide (1.2 mmoL) was dropped to 10 mL GO suspension (1.5 mg mL^{-1}) and the resulting mixture was ultra-sonicated for 5 min. Then, the mixture heated through in an autoclave for 12 h at 180 °C. Eventually, the 3D-(N)GFs were obtained by freeze drying of the prepared samples overnight.

2.4. Procedure for preparation nickel nanoparticles decorated on three-dimensional nitrogen-doped graphene-based frameworks (NiNPs@3D-(N)GFs)

3D-(N)GFs were dispersed in water (0.2 g/10.0 mL) via incorporation of an aqueous solution of $NiCl_2$ (0.2 g in 3.0 mL), followed by placing the resultant mixture in an ultrasonic bath to be sonicated for 30 min. As a result, metal ions were well-dispersed in the porosity of 3D-(N)GFs. Thereafter, the aqueous solution of $NaBH_4$ (10.5 mL, 0.01 M) increased to the resulting mixture with regard to Ni^{2+} reduction and formation of nickel nanoparticles. The obtained solution was mixed for 4 h, followed by filtering, thoroughly washing with ethanol and water and finally drying at vacuum oven for 12 h (Fig. 1). The amounts of NiNPs encapsulated on support was determined to be 11.0 wt% by atomic absorption spectroscopy (AAS) [28,29].

2.5. Synthesis of NiNPs@3D-(N)GFs/PANI hybrid

The aqueous solution of NiNPs@3D-(N)GFs with 1 mg mL^{-1} concentration was named as A. Then, the mixture of aniline (1 mL), HCl (30 mL), APS (1.2 g) and DI water (15.5 mL) were stirred in another beaker and sonicated for 5 min and the created uniform solution was named as B. Thereafter, the solution of A and B were mixed vigorously for 24 h for complete reaction. In order to eliminate the free acid, the

obtained black powders were filtered followed by twice washing with water (Fig. 2). Eventually, the NiNPs@3D-(N)GFs/PANI hybrid powders were got dry in a vacuum oven at 80 °C for 24 h.

2.6. Fabrication of NiNPs@3D-(N)GFs/PANI gas sensor

The following approached was applied for preparation of flexible gas sensor based on NiNPs@3D-(N)GFs/PANI: the polyethylene terephthalate (PET) film (1×1 cm^2) was sonicated in acetone, followed by ethanol washing and then getting dry at 50 °C. After that, the film was drop casted by 5 μL of NiNPs@3D-(N)GFs/PANI hybrid aqueous solution over it and was situated in a vacuum oven at 80 °C for 1 h. Then, flexible gas sensor was constructed by the physical vapor deposition of Au electrodes followed by was cured for 1 h in a furnace at 80 °C under nitrogen atmosphere. The manufactured NiNPs@3D-(N)GFs/PANI hybrid gas sensor is represented in Fig. 2. For comparison, flexible pure PANI gas sensor was fabricated by the same method. The thickness of the sensing film for pure PANI and NiNPs@3D-(N)GFs/ PANI hybrid was in the range of 6–10 μm. Six gas sensors were fabricated with NiNPs@3D-(N)GFs/PANI hybrid and the measured values of resistance were equal to 0.45, 0.34, 0.41, 0.33, 0.42, and 0.35 kohm, with a resistance variance of 0.132. While, the pure PANI showed an average resistance of 26.8 kohm.

2.7. Characterization

The morphology was performed by transmission electron microscopy (TEM) using a JEOL JEM-200CX. A JEOL 6700 was applied to measure scanning electron microscope (SEM) photograph. The surface areas of the materials were measured through Brunauer-Emmett-Teller (BET) method. The fourier transform infrared (FTIR) spectra was recorded on an Impact 410, Nicolet spectrometer. Raman spectra was carried out on a Nanofinder 30 confocal. X-ray photoelectron spectroscopy (XPS) was characterized with a PHI5600 Physical Electronics. The elemental composition analysis was investigated by a combustion approach, in which a thermoconductivity detector (TCD) was employed to detect the gases. The surface resistant was performed by a four-probe approach. Transport measurements were acquired in a four-terminal geometry using standard lock-in technique at ~ 17 Hz. Samples were cooled in a variable-temperature (~ 2–300 K) liquid 4He flow cryostat with the sample in vapor. Cu Kα radiation was used to obtain X-ray powder diffraction (XRD) spectra on a Philips1825 diffractometer in which silicon acted as the standard material. A lab-made closed chamber was made of steel and equipped with two electrodes Keithley 2400 LCR meter so that the resistance of sensors can be calculated. A stream of gas in the room temperature and with concentrations in the range of 1–100 ppm was fed to evaluate the responses of the sensors towards NH_3. Regarding to 100 ppm of various VOCs gasous, the selectivity test was measured at room temperature. A mass flow controller (KNH instruments) was applied to expose a constant flux of 50 cm^3 min^{-1} from dry-air with controlled humidity to various injected target gaseous. In this process, a HIH4000 and PT100 were in charge of demonstrating the temperature of sensor and relative humidity (RH%), respectively. One can calculate the changes in the sensor response S (%) via the as-blow equations:

$$S(\%) = \frac{\Delta R}{R_0} \times 100 \tag{1}$$

and

$$\Delta R = R_{gas} - R_0 \tag{2}$$

Where R_0 stands for the resistance of sensor in pure gas, and R_{gas} demonstrates the sensor resistance in the test gas. A basic square root function was applied for the calibration of response and elimination of small signal draft [30–32]. In addition, the lowered limit of detection (LOD) was calculated by the as-mentioned procedure in Supporting
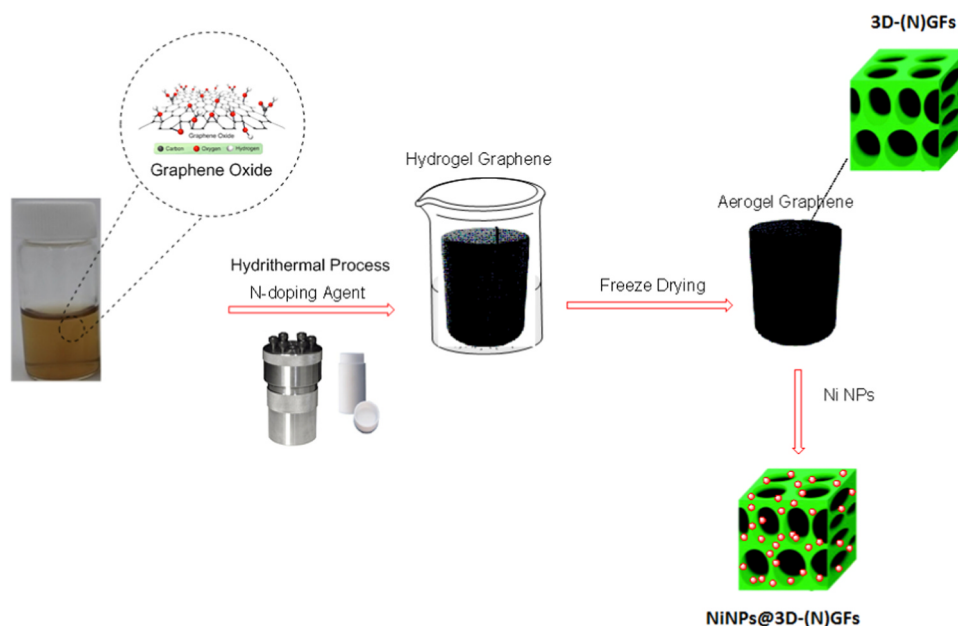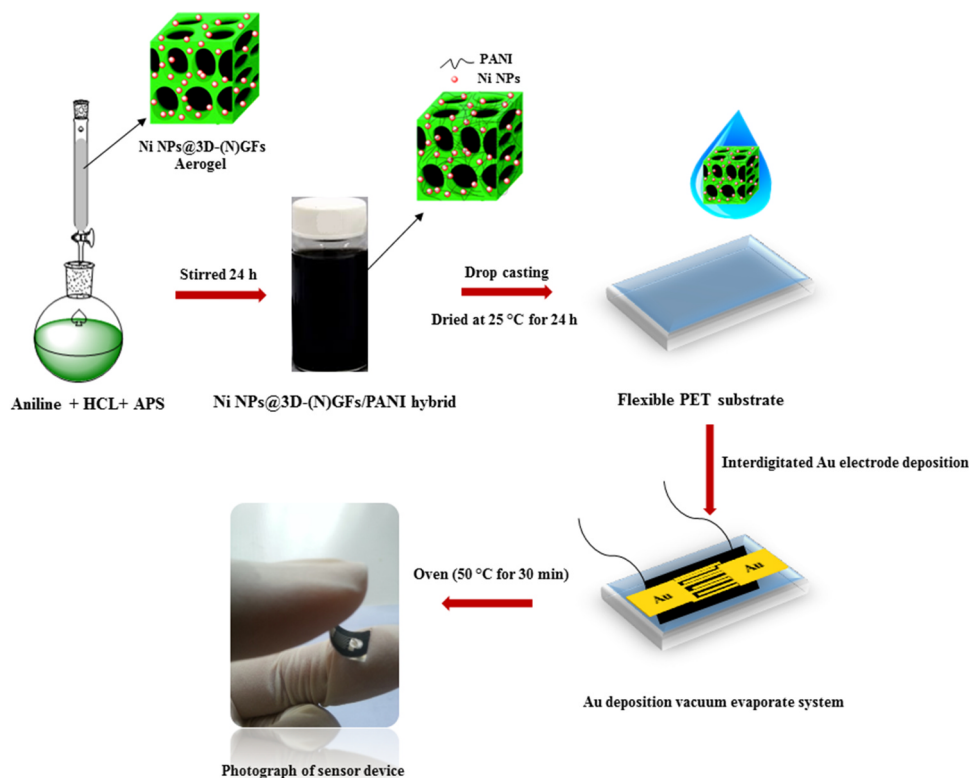
Fig. 1. Synthesis of NiNPs@3D-(N)GFs.

Fig. 2. Schematic illustration of a NiNPs@3D-(N)GFs/PANI hybrid gas sensor on flexible PET substrate.

information. Moreover, the gas response of fabricated flexible sensors towards NH_3 gas was investigated when different bending degrees were applied to PET substrate. Finally, a goniometer was employed to measure the bending angle.

3. Results and discussion

The steps of synthesizing three-dimensional nitrogen-doped graphene-based frameworks (3D-(N)GFs) are shown in Fig. 1. Typical SEM and TEM images of the synthesized large sized GO nanosheets are

demonstrated in Fig. 3(a-b), respectively. These images not only confirm the exfoliated GO nanosheets with lateral size of tens of micrometers, but also demonstrate that the exfoliated GO nanosheets are composed of single layers with a size of several micrometers.

The 3D interconnected morphology of ultrathin graphene nanosheets including porous framework has been represented in Fig. 3(c-d). Moreover, the pore size of the synthesized 3D-(N)GFs is in the range of a few hundred nanometers to several micrometers. On the other hand, the large pore volume of 3D-(N)GFs provided a large space for ammonia (NH_3) to be embedded there. In addition, the surface area is
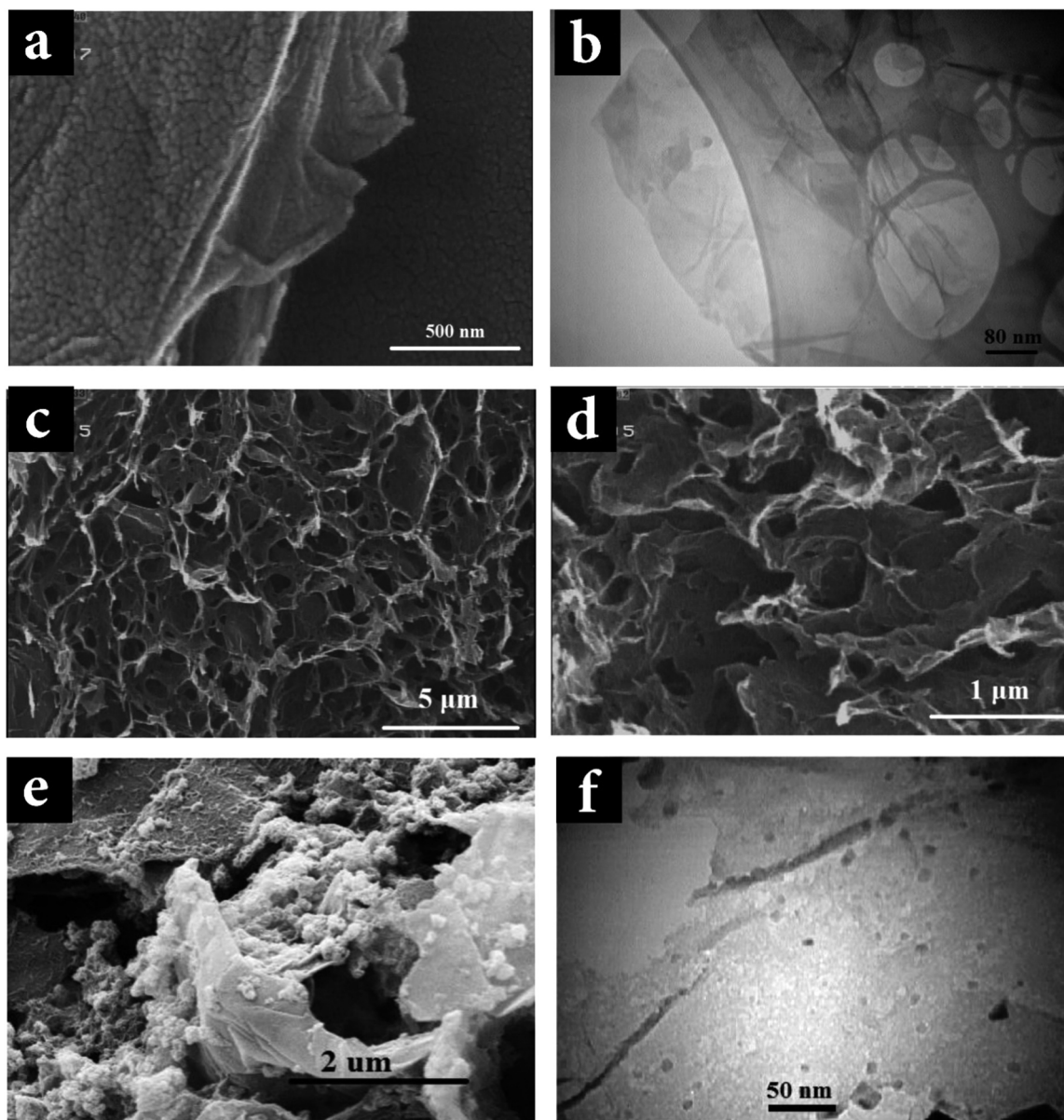
Fig. 3. (a and b) SEM and TEM images of GO, respectively. (c and d) High and low magnification SEM images of 3D-(N)GFs. (e and f) SEM and TEM images of NiNPs@3D-(N)GFs, respectively.

one of the important parameters determining the amount of adsorbed NH_3 on porous materials. Based on the Nitrogen adsorption-desorption evaluation, the typical BET surface area of 3D-(N)GFs was calculated to be about $260.0 \, m^2 \, g^{-1}$.

Both structural factors, particle size of metal nanoparticles and surface area of graphene significantly affected the nanocomposite hybrid sensitivity. The small highly-dispersed metal nanoparticles have promoted the contact level between nanocomposite hybrid and the VOC gases, thereby increasing the adsorption rate of VOC on porous substrate. Thus, small and controllable metal nanoparticles with large surface areas are of much potential in preparation of highly active sensing nanocomposite hybrid. Nickel nanoparticles were doped on 3D-(N)GFs to obtain highly active sensing materials. For this purpose, Ni^{2+} particles were added to the 3D-(N)GFs, followed by were reduced with sodium borohydride. SEM and TEM tests were performed to assess the effectiveness of immobilized Ni nanoparticles on the 3D-(N)GFs, and also to analyze the distribution of Ni nanoparticles. According to SEM and TEM images of NiNPs@3D-(N)GFs presented in Fig. 3(e-f), the Ni nanoparticles are uniformly dispersed with an average diameters of

3–8 nm on 3D-(N)GFs pores. In addition, after synthesizing NiNPs@3D-(N)GFs, the surface area was decreased to $225 \, m^2 \, g^{-1}$ showing the occupation of frameworks pores by dispersed nickel nanoparticles. In the following, the chemical composition of GO, 3D-GFs and 3D-(N)GFs was confirmed by Raman, FTIR and XRD results as shown in Fig. S1(a-c).

The components analysis of NiNPs@3D-(N)GFs was probed by X-ray energy dispersive spectrum (EDS) as presented in Fig. S1(d). As can be seen, the NiNPs@3D-(N)GFs mainly consist of C, Ni, O and N elements. In addition, the presence of Au elements is owning to the surface coating of samples with Au layers for characterizations tests.

XRD pattern of NiNPs@3D-(N)GFs is presented in Fig. S2(a). The NiNPs@3D-(N)GFs showed the higher broad diffraction peak at 25.6° as compared to its of 3D-(N)GFs at 22.6°. In addition, the existence of face centered-cubic nickel nanoparticles has been clearly exhibited [6,27,33]. As can be seen that the low d-spacing (ca. 0.34 nm) of the NiNPs@ 3D-(N)GFs is more than that of the 3D-(N)GFs (ca. 0.38 nm). The decreased d-spacing in NiNPs@3D-(N)GFs is owning to the π-π stacking of minute graphene nanosheets which is affected by embedded

Ni atoms into the conjugated carbonic structure of 3D-(N)GFs. XPS analysis was carried out to analysis the nitrogen embedding and to investigate the NiNPs doping on the synthesized NiNPs@3D-(N)GFs as presented in Fig. S2(b). The XPS spectrum of NiNPs@3D-(N)GFs shows a predominant graphitic C1s, N1s, O1s, and Ni(0) 2p at 298.4, 400, 533 and 870 eV, respectively. The high-resolution N1s spectrum of the NiNPs@3D-(N)GFs disclose the existence of third pridine-like (397.2 eV), pyrrolic (399.4 eV), and graphitic (401.7 eV) N atoms (Fig. S2(c)) [22,25,34]. Moreover, two prominent absorption bands at 865 and 882 eV regarding to Ni(0) 2p3/2 and Ni(0) 2p1/2, respectively (Fig. S2(d)), are presented in the high-resolution of Ni(0) 2p spectrum. These binding energy values are in accordance with those reported for Ni(0) oxidation states [27]. These results have proved the promising encapsulation of N and Ni atoms into the 3D-GFs.

The FTIR spectra of pure PANI and NiNPs@3D-(N)GFs/PANI hybrid are shown in Fig. S3(a). There are several main characteristic peaks in the FTIR spectrum of pure PANI which include the ones related to the stretching C=N and vibration C=C groups of the quinonoid and benzenoid units which are appeared at 1562 and 1470 cm^{-1}; the peaks attributed to the stretching mode of C-N bonds of benzenoid unit appeared at 1297 and 1240 cm^{-1}; the band at 1107 cm^{-1} which belongs to aromatic in-plane C-H bond; the shoulder and peak around 840–950 cm^{-1} is owning to vibration C-H group in 1,2,4-disubstitude benzene; the peaks appeared at 1043 and 802 cm^{-1} which are assigned to the C-Cl and C-H bands in 1,4-disubstituted benzene [17,35–37]. Although the FTIR spectrum of NiNPs@3D-(N)GFs/PANI hybrid are almost similar to those of pure PANI, all bands of the hybrid indicate small red shifts. In addition, the observed peaks in the range of 450–700 cm^{-1} have completely vanished (highlighted in red color). These results may be caused by two phenomena: exsictence of π-π interactions between NiNPs@3D-(N)GFs and PANI; as well as promising formation of NiNPs@3D-(N)GFs/PANI hybrids [9,17,38].

Typical XRD patterns of pure PANI and NiNPs@3D-(N)GFs/PANI hybrid are represented in Fig. S3(b). The pure PANI have shown three peaks at 15.2°, 20.4° and 25.4° which are assigned to the typical amorphous structure of PANI chains based on standard JCPDS values, NO 72–0634. The XRD pattern of NiNPs@3D-(N)GFs/PANI hybrid is the same as that of pure PANI. However, the slight red-shift of the peaks' position was observed owing to incorporation of NiNPs@3D-(N)GFs in the hybrids. The morphological structure of pure PANI and NiNPs@3D-(N)GFs/PANI hybrid as SEM images are presented in Fig. S3(c-d). Both pure PANI and NiNPs@3D-(N)GFs/PANI hybrid indicate regular fibrous structure in nanometers scale. In addition, all NiNPs@3D-(N)GFs are uniformly dispersed in the PANI substrate without any adverse effects on the fibrous structure of PANI. Homogenous and uniform dispersion is an important factor in improving final properties of hybrid materials [39,40]. It is worth mentioning that the porosity of fibrous structure in NiNPs@3D-(N)GFs/PANI hybrid results in short response times and pleasant reversibility towards NH₃, owning the easy diffusion of NH₃ molecules followed by its quick reaction with hybrid sensing film [17,41].

The flexible pure PANI and NiNPs@3D-(N)GFs/PANI hybrid gas sensors were exposed to 100 ppm NH₃ at 25 °C and 57% RH repeatedly in three cycles, and their dynamic responses are shown in Fig. 4(a-b), respectively. The resistance of both sensors has decreased rapidly by placing the sensor into the vessel containing 100 ppm NH₃, and has recovered to the initial value after removing out, and exposing to air. It is clearly seen that NiNPs@3D-(N)GFs/PANI hybrid exhibits a typical p-type semiconductor property. Fig. 4(c-d) present the initial resistances of the flexible pure PANI and NiNPs@3D-(N)GFs/PANI hybrid gas sensors towards various concentrations of NH₃ at 25 °C and 57% RH, respectively. The resistance of flexible pure PANI sensor is equal to 37.82 kohm at 300 ppm of NH₃, which is much higher than that of the flexible NiNPs@3D-(N)GFs/PANI hybrid one (1.3 kohm). The flexible pure PANI present the conductivity of 37.2 S cm^{-1}, while it's of NiNPs@3D-(N)GFs/PANI hybrid sensing film are and 97.5 S cm^{-1}. This

is caused by the significant increment in the charge carrier concentration owning to NiNPs@ 3D-(N)GFs existence. These results indicate the successful modification of PANI with NiNPs@ 3D-(N)GFs. The small change in the resistance of sensors may be assigned to the adsorption and desorption of NH₃ molecules on the hybrid sensing film, which will further be discussed later. The quantitative responses of flexible pure PANI and NiNPs@ 3D-(N)GFs/PANI hybrid gas sensors were measured towards various NH₃ concentrations in the range of 1–100 ppm and 1–1000 ppm at 25 °C and 57% RH, as shown in Fig. S4(c-d). Regarding to 100 ppm NH₃, the sensitivity of the flexible NiNPs@3D-(N)GFs/PANI hybrid gas sensors is about 10.1% and 89.5%, respectively. Moreover, a value of 750.2 at 1000 ppm NH₃ was found as the highest response of NiNPs@3D-(N)GFs/PANI hybrid gas sensor in comparison to pure PANI one (~ 53.5).

Response time, the period of time in which the detected gas reaches to 90% equilibrium after injection; and recovery time, the required time to achieve 90% of final equilibrium after gas removal; are considered as two additional important parameters in gas sensors. The response and recovery times of flexible pure PANI gas sensor in the case of exposure to 10 ppm NH₃ were equal to 183 and 77 s, respectively, while these values for flexible NiNPs@3D-(N)GFs/PANI hybrid gas sensor were measured to be equal to 95 and 32 s, respectively. Moreover, based on Fig. S4(a-b), the room temperature (25 °C) and humidity of 57% is the suitable practical condition for the flexible NiNPs@3D-(N)GFs/PANI hybrid gas sensor in order to detect NH₃. In addition, it is noteworthy to mention that the LOD of the NiNPs@3D-(N)GFs/PANI hybrid gas sensor was calculated to be as low as 45 ppb, which was much lower than that of the pure PANI gas sensor (10 ppm). According to the American Conference of Governmental Industrial Hygienists, a threshold exposure limit of 100 ppb NH₃ is recommended. Apparently, the calculated LOD of our sensor is far below the threshold exposure limit. The ability to detect NH₃ with low concentration indicates the potential practical applicability of this gas sensor. It should be noted that sensing performances of the flexible gas senor based on NiNPs@3D-(N)GFs/PANI hybrid are much better than the previously reported NH₃ gas sensors based on PANI based materials as well as commercial NH₃ ones. A detailed comparison of the gas sensors is given in Table 1.

In addition to sensitivity, selectivity are another vital indicators in design and application of gas sensors. Thus, the selectivity of the flexible pure PANI and NiNPs@3D-(N)GFs/PANI hybrid gas sensors to various VOC gases with 100 ppm concentration at 25 °C and 57% RH, is represented in Fig. 5(a). After exposure to 100 ppm of NH₃, toluene, methanol, acetone, ethanol, chlorobenzene, and propanol, the sensitivity of flexible NiNPs@3D-(N)GFs/PANI hybrid gas sensor was obtained 89.5%, 0.63%, 0.52%, 0.45%, 0.42%, 0.57%, and 0.41%, respectively, suggesting a higher selectivity to NH₃ in comparison with other VOC gases.

The bending effect of PET substrate on NH₃ sensing of flexible pure PANI and NiNPs@3D-(N)GFs/PANI hybrid gas sensors under exposure to 100 ppm NH₃, is shown in Fig. 5(b) versus variations of the bending angle in the range of 0–80°. The sensitivity of both sensors was increased 3interestingly with the bending angle so that the responses of flexible pure PANI and NiNPs@3D-(N)GFs/PANI hybrid gas sensors at a bending angle of 80° were about 1.5 and 3 times higher than those of both sensors at 0° banding angle, respectively. The improved swelling process can be considered as the leading cause in enhanced NH₃ sensing response by bending angle [9,25]. Under this condition, (i.e., swelling) NH₃ molecules can easier diffuse into the NiNPs@3D-(N)GFs/PANI layer under bending extension. Under such a situation, electron hopping becomes more challenging as the distance between PANI chains increases. In the case of NiNPs@3D-(N)GFs/PANI, NiNPs@3D-(N)GFs embedded into polymer matrix acts as conductive pathways, favoring electron hopping. The swelling process can lead to dissociation of the NiNPs@3D-(N)GFs, thereby disrupting conductive pathways. Longer distance between PANI chains, together with lower conductive pathways results in considerable increase in resistance of the NiNPs@3D-
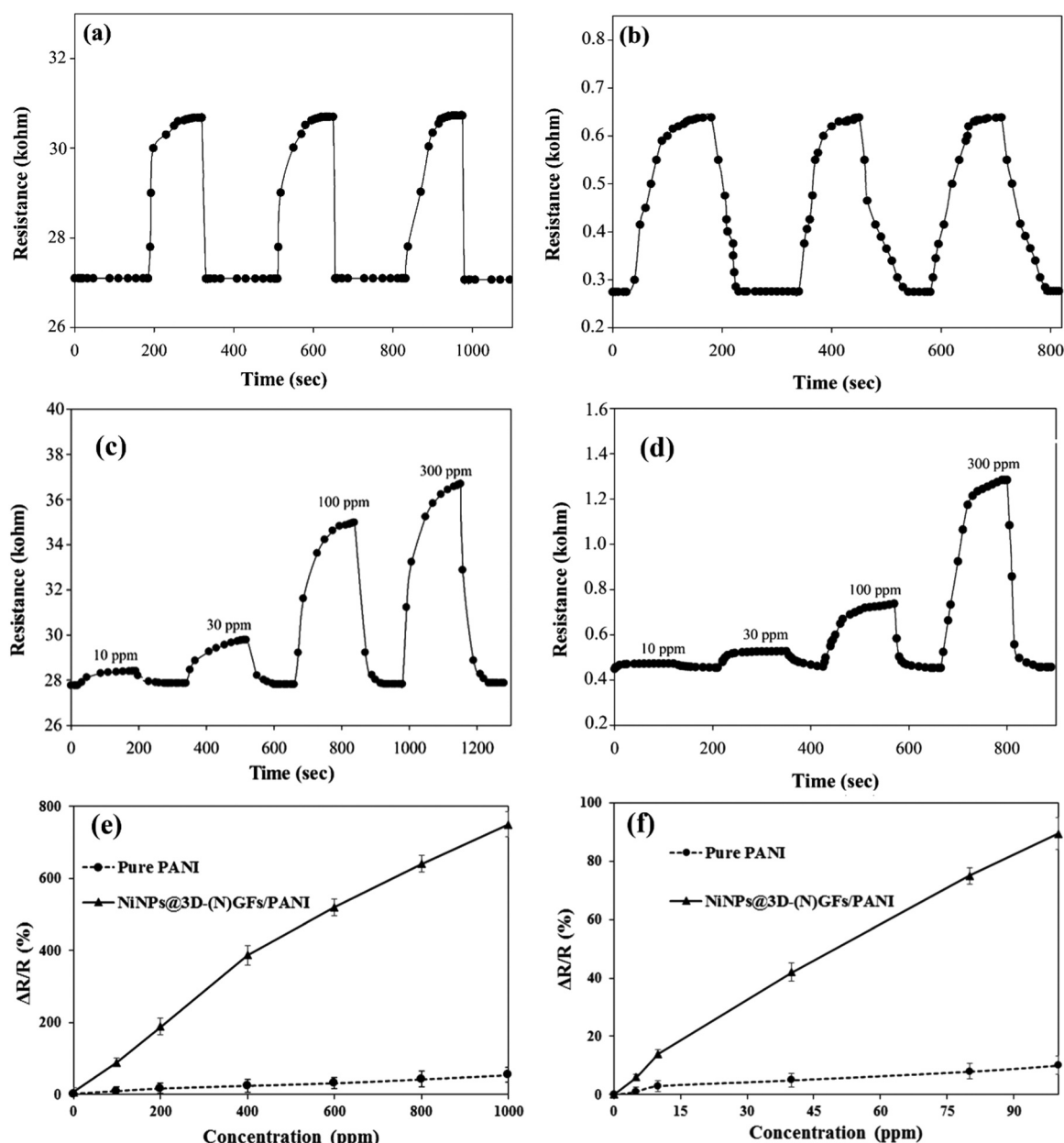
Fig. 4. (a and b) Dynamic responses of flexible pure PANI, and NiNPs@3D-(N)GFs/PANI hybrid gas sensors to 100 ppm NH$_3$ at 25 °C and 57% RH repeatedly in three cycles, respectively. (c and d) Dynamic reposes of flexible pure PANI, and NiNPs@3D-(N)GFs/PANI hybrid gas sensors versus time upon exposure to 10–300 ppm NH$_3$ at 25 °C and 57% RH, respectively. (e and f) Quantitative responses of flexible pure PANI and NiNPs@3D-(N)GFs/PANI hybrid gas sensors at 25 °C and 57% RH regarding to various concentrations NH$_3$: 1–1000 ppm, and 1–100 ppm, respectively.

(N)GFs/PANI sensor by NH$_3$ and consequently enhanced NH$_3$ response. The resistance of NiNPs@3D-(N)GFs/PANI sensor is completely recovered to its baseline after polymer de-swelling/shrinkage by purge of or long-term exposure to dry air.

One can attribute the improved NH$_3$ sensitivity of flexible NiNPs@ 3D-(N)GFs/PANI hybrid gas sensors to the following four reasons:

I. PANI nanoparticles are anchored on the surface of NiNPs@3D-(N)GFs sheets, providing a large specific surface area and porous structure for the hybrid which is of great benefit to NH$_3$ adsorption and deprotonation at the interface of hybrid [47,48]. In other words, according to nitrogen adsorption–desorption analysis, BET surface area was found to be 260.0 m^2 g^{-1} for 3D-(N)GFs which indicates the high surface area of support to immobilize NiNPs as active catalytic sites. After synthesizing NiNPs@3D-(N)GFs, the surface area was

decreased to 225 m^2 g^{-1}, indicating the occupation of frameworks pores by dispersed nickel nanoparticles. In the case of NiNPs@3D-(N)GFs/PANI, the surface area was increased to 454 m^2 g^{-1} which suggests the presence of PANI between the graphene sheets and consequently reducing the layer-to-layer restacking. The adsorption/desorption phenomena and deprotonation at the interface are the main mechanisms of sensing process. Hence, in order to achieve high sensing performance for gas sensing materials, it is very important to fabricate a sensor with as large specific surface area as possible. When NiNPs@3D-(N)GFs/PANI layers are exposed to the NH$_3$ gas, the number of charge carriers will be decreased due to the electron withdrawal nature of absorbed water, and co-doped nitrogen and nickel nanoparticles on hybrid structure, as well as available free oxygen which induce hole-like carriers, causing an increase in resistance, thereby enhancing NH$_3$ detection [49,50].

Table 1
Detailed sensitivity results of various gas sensors to NH₃.

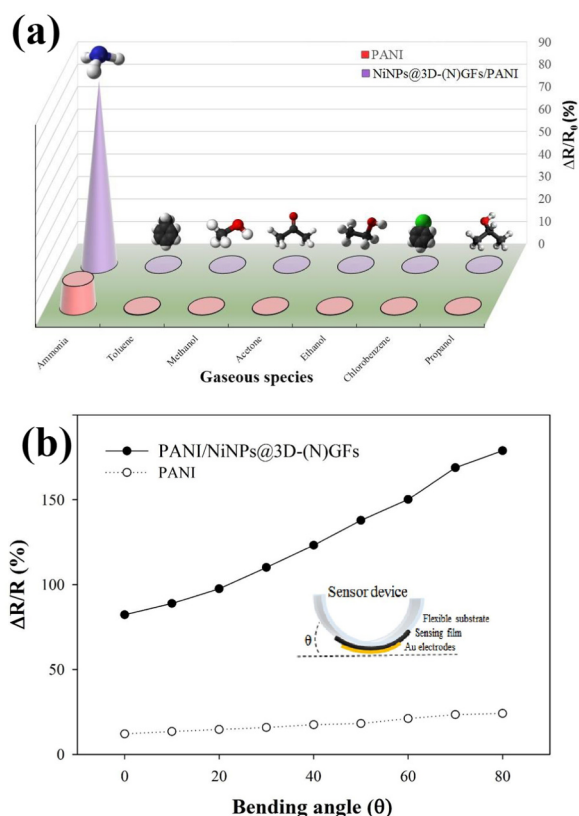| Authors	Sensitivity (%)	Response time (s)	Recovery time (s)	Detection range (ppm)	Material	Measured temperature (°C)
Our Work	89.5 (100 ppm), 750 0.2 (1000 ppm)	95	32	1–1000	NiNPs@3D-(N)GFs/PANI hybrid	25
GPro 500 (Mettler Toledo)	101 (100 ppm)	< 4	–	0–10,000	Tunable Diode Laser	0–250
NH/NH2 (Aeroqual Limited)	450 (1000 ppm)	30	< 120	0–1000		0–40
Nasrollah Gavgani et al. [22]	42.3 (100 ppm), 385 (1000 ppm)	115	44	1–1000	S, N: GQDs/PANI hybrid	25
Nylander et al. [42]	30 (10,000 ppm)	< 60	–	–	Commercial available conducting polymer: pyrrole black	25
Dehsari et al. [43]	8 (50 ppm), 91 (1000 ppm)	150	60	1–1000	CuTSPc@3D-(N)GFs/PEDOT-PSS	25
Kwon et al. [44]	2.1 (5 ppm), 24 (100 ppm)	< 1	30	5–100	PEDOT nanotube	25
Seekaew et al. [9]	0.9 (5 ppm), 7 (1000 ppm)	180	–	5–1000	Graphene/PEDPT-PSS	25
Jian et al. [45]	0.1 (2 ppm), 33 (300 ppm)	12	18	2–300	SWCNTs/PEDOT-PSS	25
Yoo et al. [11]	0.015 (20 ppm), 0.075 (100 ppm)	100	700	0–100	pf-MWCNT/PANI	25
Tai et al. [41]	1.67 (23 ppm), 5.55 (117 ppm)	18	58	23–141	PANI/TiO₂	25
Hong et al. [3]	0.14 (20 ppm), 0.2 (100 ppm)	14	148	20–2000	Palladium/Polypyrrole	25
Crowley et al. [1]	0.24 (100 ppm)	90	90	1–100	Inkjet-printed PANI	80
Sengupta et al. [46]	2.3 (100 ppm)	120	300	100	PANI	25

Fig. 5. (a) Selectivity and (b) flexibility of the pure PANI and NiNPs@3D-(N)GFs/PANI hybrid gas sensors upon exposure to 100 ppm NH₃ at 25 °C in 57% RH.

(II) At room temperature, a high carrier mobility is provided by NiNPs@3D-(N)GFs sheets, causing a rapid rise in the hybrid resistance which decreases the response time of hybrid regarding to the NH₃ gas [51,52]. On the other hand, based on transport measurements, the electron mobility for NiNPs@3D-(N)GFs/PANI increased to $1,100,000\ cm^{-2}\ V^{-1}\ s^{-1}$ as compared to its of NiNPs@3D-(N)GFs ($\sim 650,000\ cm^{-2}\ V^{-1}\ s^{-1}$) and 3D-(N)GFs ($\sim 430,000\ cm^{-2}\ V^{-1}\ s^{-1}$). Therefore, Stable π-π interaction between the conjugated PANI and NiNPs@ 3D-(N)GFs result in more free electron transfer through NH₃ detection, which therefor improve the sensitivity of hybrid [1,49,53].

4. Conclusion

The NiNPs@3D-(N)GFs/PANI hybrid were fabricated through simple, in-situ oxidative polymerization. The NH₃ gas sensors were successfully fabricated based on loading pure PANI and NiNPs@3D-(N)GFs/PANI hybrid on flexible PET film. Among the specimens prepared, the highest value of sensitivity (750.2) as well as fastest response and recovery times (95 s and 32 s, respectively) towards 1000 ppm NH₃ at room temperature, were observed in the flexible NiNPs@3D-(N)GFs/PANI hybrid gas sensor. In addition, the sensitivity of both flexible gas sensors was significantly grown with bending angle increment. The improvement of sensitivity performance for the NiNPs@3D-(N)GFs/PANI hybrid was attributed to the increased charge transfer due to intorduction of embedded Ni and N atoms on conjugated graphenic structure as well as synergistic π-π interaction between the NiNPs@3D-(N)GFs and PANI. Therefore, the NiNPs@3D-(N)GFs/PANI hybrid fulfil great pledge for detection of NH₃.

Appendix A. Supporting information

Supplementary data associated with this article can be found in the online version at doi:10.1016/j.talanta.2019.01.060

References

[1] K. Crowley, et al., Fabrication of an ammonia gas sensor using inkjet-printed polyaniline nanoparticles, Talanta 77 (2) (2008) 710–717.

[2] M. Gautam, A.H. Jayatissa, Ammonia gas sensing behavior of graphene surface decorated with gold nanoparticles, Solid-State Electron. 78 (2012) 159–165.

[3] L. Hong, Y. Li, M. Yang, Fabrication and ammonia gas sensing of palladium/polypyrrole nanocomposite, Sens. Actuators B: Chem. 145 (1) (2010) 25–31.

[4] S. Mao, et al., Tuning gas-sensing properties of reduced graphene oxide using tin oxide nanocrystals, J. Mater. Chem. 22 (22) (2012) 11009–11013.

[5] M. Suchea, et al., Low temperature indium oxide gas sensors, Sens. Actuators B: Chem. 118 (1) (2006) 135–141.

[6] J. Wang, P. Yang, X. Wei, High-performance, room-temperature, and no-humidity-impact ammonia sensor based on heterogeneous nickel oxide and zinc oxide nanocrystals, ACS Appl. Mater. Interfaces 7 (6) (2015) 3816–3824.

[7] H. Kebiche, et al., Relationship between ammonia sensing properties of polyaniline nanostructures and their deposition and synthesis methods, Anal. Chim. Acta 737 (2012) 64–71.

[8] M. Matsuguchi, et al., Effect of NH_3 gas on the electrical conductivity of polyaniline blend films, Synth. Met. 128 (1) (2002) 15–19.

[9] Y. Seekaew, et al., Low-cost and flexible printed graphene–PEDOT: PSS gas sensor for ammonia detection, Org. Electron. 15 (11) (2014) 2971–2981.

[10] L. Zhihua, et al., Fast response ammonia sensor based on porous thin film of polyaniline/sulfonated nickel phthalocyanine composites, Sens. Actuators B: Chem. 226 (2016) 553–562.

[11] K.-P. Yoo, et al., Effects of O_2 plasma treatment on NH_3 sensing characteristics of multiwall carbon nanotube/polyaniline composite films, Sens. Actuators B: Chem. 143 (1) (2009) 333–340.

[12] F.A. Tabar, F. Sharif, S. Mazinani, Preparation and electrochemical performance of a novel three dimensional structure of polyaniline hollow fibers decorated by graphene, Polymer 154 (2018) 80–89.

[13] S. Baseghi, et al., Lightweight high-density polyethylene/carbonaceous nanosheets microcellular foams with improved electrical conductivity and mechanical properties, J. Mater. Sci. 50 (14) (2015) 4994–5004.

[14] J.N. Gavgani, H. Adelnia, M.M. Gudarzi, Intumescent flame retardant polyurethane/reduced graphene oxide composites with improved mechanical, thermal, and barrier properties, J. Mater. Sci. 49 (1) (2014) 243–254.

[15] M. Soheilmoghaddam, et al., Development of ethylene-vinyl acetate composites reinforced with graphene platelets, Macromol. Mater. Eng. 302 (2) (2017) 1600260.

[16] M.A. Worsley, et al., Synthesis of graphene aerogel with high electrical conductivity, J. Am. Chem. Soc. 132 (40) (2010) 14067–14069.

[17] Z. Wu, et al., Enhanced sensitivity of ammonia sensor using graphene/polyaniline nanocomposite, Sens. Actuators B: Chem. 178 (2013) 485–493.

[18] R. Ghosh, et al., Highly sensitive large-area multi-layered graphene-based flexible ammonia sensor, Sens. Actuators B: Chem. 205 (2014) 67–73.

[19] J.N. Gavgani, et al., Highly sensitive and flexible ammonia sensor based on S and N co-doped graphene quantum dots/polyaniline hybrid at room temperature, Sens. Actuators B: Chem. (2016).

[20] X. Dong, et al., 3D graphene foam as a monolithic and macroporous carbon electrode for electrochemical sensing, ACS Appl. Mater. Interfaces 4 (6) (2012) 3129–3133.

[21] F. Yavari, et al., High sensitivity gas detection using a macroscopic three-dimensional graphene foam network, Sci. Rep. 1 (2011) 166.

[22] J.N. Gavgani, et al., Highly sensitive and flexible ammonia sensor based on S and N co-doped graphene quantum dots/polyaniline hybrid at room temperature, Sens. Actuators B: Chem. 229 (2016) 239–248.

[23] J.N. Gavgani, et al., Lightweight flexible polyurethane/reduced ultralarge graphene oxide composite foams for electromagnetic interference shielding, RSC Adv. 6 (33) (2016) 27517–27527.

[24] D.S. Yu, et al., Effects of covalent surface modifications on the electrical and electrochemical properties of graphene using sodium 4-aminoazobenzene-4′-sulfonate, Carbon 54 (2013) 310–322.

[25] Z.-H. Sheng, et al., Electrochemical sensor based on nitrogen doped graphene: simultaneous determination of ascorbic acid, dopamine and uric acid, Biosens. Bioelectron. 34 (1) (2012) 125–131.

[26] S.H. Aboutalebi, et al., Spontaneous formation of liquid crystals in ultralarge graphene oxide dispersions, Adv. Funct. Mater. 21 (15) (2011) 2978–2988.

[27] N.R. Gleason, F. Zaera, Thermal conversion of 2-propyl iodide on O/Ni (100): changes in product distribution with varying oxygen coverages, J. Catal. 169 (1) (1997) 365–381.

[28] Q. Xu, M. Chandra, Catalytic activities of non-noble metals for hydrogen generation from aqueous ammonia–borane at room temperature, J. Power Sources 163 (1) (2006) 364–370.

[29] M. Mahyari, A. Shaabani, Nickel nanoparticles immobilized on three-dimensional nitrogen-doped graphene as a superb catalyst for the generation of hydrogen from the hydrolysis of ammonia borane, J. Mater. Chem. A 2 (39) (2014) 16652–16659.

[30] N. Strömberg, A. Hakonen, Plasmophore sensitized imaging of ammonia release from biological tissues using optodes, Anal. Chim. Acta 704 (1–2) (2011) 139–145.

[31] N. Strömberg, S. Hulth, Assessing an imaging ammonium sensor using time correlated pixel-by-pixel calibration, Anal. Chim. Acta 550 (1–2) (2005) 61–68.

[32] N. Strömberg, S. Hulth, Time correlated pixel-by-pixel calibration for quantification and signal quality control during solute imaging, Sens. Actuators B: Chem. 115 (1) (2006) 263–269.

[33] M. Jiang, et al., Effect of $Ni2+$ as a codopant on the structure, morphology, and conductivity of nanostructured polyaniline, J. Appl. Polym. Sci. 121 (6) (2011) 3439–3445.

[34] Z.S. Wu, et al., Three-dimensional nitrogen and boron co-doped raphene for High-performance all-solid-state supercapacitors, Adv. Mater. 24 (37) (2012) 5130–5135.

[35] A.V. Murugan, T. Muraliganth, A. Manthiram, Rapid, facile microwave-solvothermal synthesis of graphene nanosheets and their polyaniline nanocomposites for energy strorage, Chem. Mater. 21 (21) (2009) 5004–5006.

[36] J. Tang, et al., Infrared spectra of soluble polyaniline, Synth. Met. 24 (3) (1988) 231–238.

[37] M. Trchová, et al., FTIR spectroscopic and conductivity study of the thermal degradation of polyaniline films, Polym. Degrad. Stab. 86 (1) (2004) 179–185.

[38] W. Si, et al., Electrodeposition of graphene oxide doped poly (3, 4-ethylenedioxythiophene) film and its electrochemical sensing of catechol and hydroquinone, Electrochim. Acta 85 (2012) 295–301.

[39] M. Soheilmoghaddam, et al., Bionanocomposite regenerated cellulose/single-walled carbon nanotube films prepared using ionic liquid solvent, Cellulose 24 (2) (2017) 811–822.

[40] H. Adelnia, et al., Gas permeability and permselectivity properties of ethylene vinyl acetate/sepiolite mixed matrix membranes, Sep. Purif. Technol. 146 (2015) 351–357.

[41] H. Tai, et al., Fabrication and gas sensitivity of polyaniline–titanium dioxide nanocomposite thin film, Sens. Actuators B: Chem. 125 (2) (2007) 644–650.

[42] C. Nylander, M. Armgarth, I. Lundström, An ammonia detector based on a conducting polymer, Anal. Chem. Symp. Ser. (1983).

[43] H.S. Dehsari, et al., Copper (II) phthalocyanine supported on three-dimensional nitrogen-doped graphene/PEDOT-PSS nanocomposite as highly selective and sensitive sensor for ammonia detection at room temperature, RSC Adv. (2015).

[44] O.S. Kwon, et al., Novel flexible chemical gas sensor based on poly (3, 4-ethylenedioxythiophene) nanotube membrane, Talanta 82 (4) (2010) 1338–1343.

[45] J. Jian, et al., Gas-sensing characteristics of dielectrophoretically assembled composite film of oxygen plasma-treated SWCNTs and PEDOT/PSS polymer, Sens. Actuators B: Chem. 178 (2013) 279–288.

[46] P.P. Sengupta, P. Kar, B. Adhikari, Influence of dopant in the synthesis, characteristics and ammonia sensing behavior of processable polyaniline, Thin Solid Films 517 (13) (2009) 3770–3775.

[47] S. Deng, et al., Reduced graphene oxide conjugated Cu2O nanowire mesocrystals for high-performance NO2 gas sensor, J. Am. Chem. Soc. 134 (10) (2012) 4905–4917.

[48] S. Bai, et al., Ultrasensitive room temperature NH_3 sensor based on a graphene–polyaniline hybrid loaded on PET thin film, Chem. Commun. 51 (35) (2015) 7524–7527.

[49] X. Huang, et al., Reduced graphene oxide–polyaniline hybrid: preparation, characterization and its applications for ammonia gas sensing, J. Mater. Chem. 22 (42) (2012) 22488–22495.

[50] F. Yavari, et al., High sensitivity gas detection using a macroscopic three-dimensional graphene foam network, Sci. Rep. (2011) 1.

[51] X. Huang, et al., Graphene-based composites, Chem. Soc. Rev. 41 (2) (2012) 666–686.

[52] R.K. Joshi, et al., Graphene films and ribbons for sensing of O2, and 100 ppm of CO and NO2 in practical conditions, J. Phys. Chem. C 114 (14) (2010) 6610–6613.

[53] J.N. Gavgani, et al., A room temperature volatile organic compound sensor with enhanced performance, fast response and recovery based on N-doped graphene quantum dots and poly (3, 4-ethylenedioxythiophene)–poly (styrenesulfonate) nanocomposite, RSC Adv. 5 (71) (2015) 57559–57567.